PCCP

Cite this: *Phys. Chem. Chem. Phys.*, 2012, **14**, 5945–5952

www.rsc.org/pccp

PAPER

Layered $Na_{0.71}CoO_2$: a powerful candidate for viable and high performance Na-batteries†

Massimiliano D'Arienzo,*[a] Riccardo Ruffo,*[a] Roberto Scotti,[a] Franca Morazzoni,[a] Claudio Maria Mari[a] and Stefano Polizzi[b]

Received 5th March 2012, Accepted 6th March 2012
DOI: 10.1039/c2cp40699c

The present study reports on the synthesis and the electrochemical behavior of $Na_{0.71}CoO_2$, a promising candidate as cathode for Na-based batteries. The material was obtained in two different morphologies by a double-step route, which is cheap and easy to scale up: the hydrothermal synthesis to produce Co_3O_4 with tailored and nanometric morphology, followed by the solid-state reaction with NaOH, or alternatively with Na_2CO_3, to promote Na intercalation. Both products are highly crystalline and have the P2-$Na_{0.71}CoO_2$ crystal phase, but differ in the respective morphologies. The material obtained from Na_2CO_3 have a narrow particle length (edge to edge) distribution and 2D platelet morphology, while those from NaOH exhibit large microcrystals, irregular in shape, with broad particle length distribution and undefined exposed surfaces. Electrochemical analysis shows the good performances of these materials as a positive electrode for Na-ion half cells. In particular, $Na_{0.71}CoO_2$ thin microplatelets exhibit the best behavior with stable discharge specific capacities of 120 and 80 mAh g^{-1} at 5 and 40 mA g^{-1}, respectively, in the range 2.0–3.9 V *vs.* Na^+/Na. These outstanding properties make this material a promising candidate to construct viable and high-performance Na-based batteries.

Introduction

Lithium ion batteries dominate the market of secondary power sources for wireless electronic equipment as they offer both high energy and good power density. Today, about 100 million lithium ion cells are produced monthly with a consumption of about 1000 tons of cathode materials. The strategic market of the automotive industry is looking to the lithium ion system as a power source for the next generation of Hybrid Electric Vehicles (HEVs) and for the future development of full electric cars. In this context, a new and unprecedented issue stands out: the massive consumption of lithium sources which could limit the future dreams of large urban air depollution and better fuel management. In fact recent calculations have pointed out that the production of Li_2CO_3 is currently about half of what would be needed to convert all cars every year produced (about 50 million) into HEVs (with an electric motor powered by a 7 kWh battery) and the demand will become astronomical considering that full electric vehicles require an onboard battery of around 40 kWh.[1] A deep evaluation on the effective availability of lithium raw materials concerns geologists (see for example the debate between R. Keith Evans and William Tahil[2]) and it is beyond the scope of the present paper; however, no doubt that the cost of lithium is increasing, and the strong future demand will make the situation even dimmer. For instance, the price of Li_2CO_3 exported from Chile increased threefold in the five-year period 2003–2008.[3]

A possible solution to the above reported drawbacks is the development of different battery systems, as recently reported by several research.[4] In this framework, growing interest lies in the sodium based systems, which were already investigated at the early stage of lithium ion technology, but after the commercialization of the first Sony battery (1990), have been almost totally abandoned. Lithium has three times larger specific capacity than sodium (3.86 *vs.* 1.08 Ah g^{-1}, respectively), but only one-tenth of this capacity is used at the battery anode and one-twentieth at the cathode. Cost and natural abundance, which are not favorable to the lithium future, are promising in the case of sodium because Na raw material (NaCl) has wider distribution than Li on the earth's crust (75% of primary lithium sources are estimated to be in South America).

The growth of a sodium based technology implies the development of electrode materials which can react in a fast and reversible way with sodium ions.[5] Although the larger Na^+ ionic radius compared to Li^+ (0.98 *vs.* 0.68 Å, respectively) might be a crucial obstacle to overcome because the high Na^+ diffusion coefficient may negatively affect the reaction kinetic,

[a] *Department of Materials Science, University of Milano Bicocca, via R. Cozzi 53, I-20125 Milan, Italy. E-mail: massimiliano.darienzo1@unimib.it, riccardo.ruffo@unimib.it*
[b] *Dipartimento di Scienze Molecolari e Nanosistemi, Università Ca' Foscari Venezia, via Torino 155/b, I-30172 Venezia, Italy*

† Electronic supplementary information (ESI) available: Details on the EDX analysis performed on $Na_{0.71}CoO_2$ phases are reported in Fig. S1. See DOI: 10.1039/c2cp40699c

the barriers for Na^+ migration can potentially be lower than that for Li^+ migration in some particular layered structures. This behavior has been recently demonstrated by computational studies.[6]

The above results clearly indicate sodium ion intercalation compounds as really promising electrode materials for the sodium based batteries. Several structures have been proposed right now, especially in the last few years: NASICON,[7,8] alluaudite phases,[9] olivines,[10,11] and tunnel oxides.[12–17]

The Na analogous of lithiated mixed oxides, which are commonly used as positive electrode materials in lithium based batteries, are seldom investigated.[13,16,17] Na_xCoO_2 was first studied back in the 1980's[18–20] as a rechargeable electrode, and its structural behavior during the sodium intercalation and de-intercalation was described in a recent seminal paper.[21] P2-Na_xCoO_2 ($x \cong 0.7$) (for the nomenclature of these phases see ref. 21) is a p-type oxide and its crystalline structure changes with the sodium content, assuming the γ-phase in the range $x = 0.65$–0.74. This phase displays hexagonal lattice consisting of layers of edge-sharing CoO_6 octahedrons, separated by sodium ions in two different crystallographic sites (see inset of Fig. 1). These adjacent sites are too close considering the Na^+ ionic radius and therefore cannot be occupied simultaneously, leading to the presence of vacant positions in the interslab space. Slight changes in Na^+ ion amount (1 or 2%) can induce a new cation distribution and structural rearrangements even at room temperature. Therefore the sodium content plays a key role in determining the electrochemical properties of the system.[21]

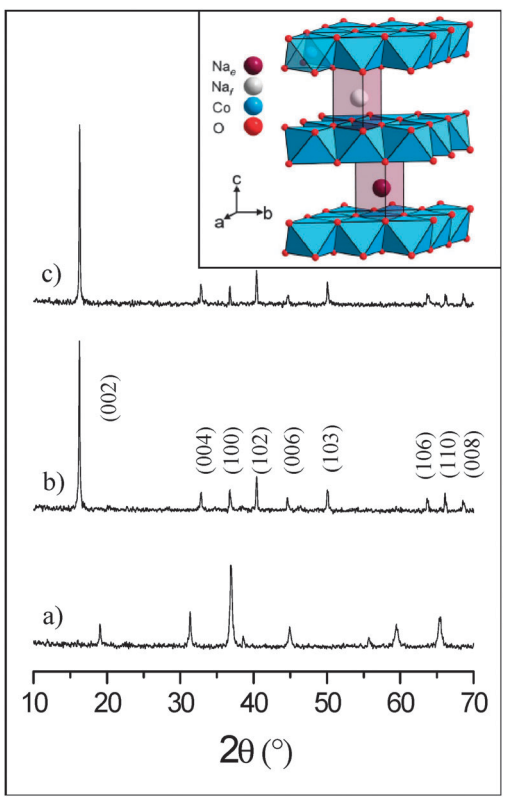

Fig. 1 XRD patterns of (a) Co_3O_4 hydrothermal nanocrystals, (b) $Na_{0.71}CoO_2$ (II) and (c) $Na_{0.71}CoO_2$ (I). The inset shows the structure of the P2-Na_xCoO_2 phases. Na_e and Na_f depict two sodium ions in two different crystallographic sites (Reprinted with permission from R. Berthelot, D. Carlier and C. Delmas, *Nat. Mater.* 2011, **10**, 74. Copyright 2010 Nature Publishing Group).

Although several electrochemical characterizations have already been made, further investigations on P2-$Na_{0.7}CoO_2$ are needed to fully understand its potential application as battery material. A brief description of the electrochemical data available for this phase is reported hereafter. In 1981, Delmas *et al.*[18] studied the Na^+ intercalation and deintercalation in the solid state obtained Na_xCoO_2 with different starting compositions and reported the first potential/composition profile during the first cycle. The P2-phase profile showed reversible behavior between 2.0 and 3.5 V *vs.* Na^+/Na, a change in composition around $\Delta x = 0.35$ in Na_xCoO_2 with a corresponding specific capacity of about 85 mAh g^{-1}. The same group more recently attempted deeper investigation on the structure–property relationship,[21] however in both cases no data are reported about the use of the material for more cycles. In 1988 Shacklette *et al.*[20] showed the first cyclability data for several Na_xCoO_2 phases (P2 and P3) obtained by solid state reaction. The best behavior in terms of capacity retention was displayed by the P2 phase with a projected capacity fading by 50% after 1000 cycles at low current. However, the measurements were obtained in a reduced potential range (1.5–3.3 V *vs.* Na^+/Na) and no data were reported on the material specific capacity. In 1993 Ma *et al.*[23] used the same solid state obtained P2-$Na_{0.7}CoO_2$ in a battery using metallic sodium or $Na_{15}Pb_4$ as the counter electrode and a solid-polymer electrolyte. The measurements were performed at 90 °C showing promising results, but once again, data about the material specific capacity upon cycling were missing (authors claimed that the initial capacity was corresponding to about $x = 0.6$ in Na_xCoO_2, *i.e.* 150 mAh g^{-1}). Recently, Bhide and Hariharan[24] tried to correlate the material morphology with its electrical and electrochemical properties. In particular, they prepared P2-$Na_{0.71}CoO_2$ by three different routes: solid-state reaction, sol–gel condensation by acetate precursors, and high energy ball-milling procedure followed by short thermal treatment. The electrochemical characterization was performed in a cell using metallic Na as the counter electrode and plasticized polymer electrolyte; the cell was only discharged from OCV to 1.75 V *vs.* Na^+/Na without any further characterization and no data about the specific capacity were reported. The best discharge properties were observed in cells with the cathode materials prepared by the sol–gel route. This was related to the small particle size and to the large surface area of the sol–gel obtained mixed oxide, both favoring the stability of the electrode–electrolyte interface and thereby the discharge properties.[24]

In this inhomogeneous and incomplete scenario, the aim of the present paper is to report, for the first time, a detailed electrochemical analysis of the P2-$Na_{0.7}CoO_2$ in half cell *vs.* metallic Na, through cyclic voltammetry measurements, potential/capacity profiles and cyclability data at different current rates. Moreover the relations among the synthesis procedure, the material morphology and the electrochemical properties were investigated, in order to lay the groundwork for a rationale design of these materials.

Two different samples were prepared starting from the same hydrothermal nanometric Co_3O_4 precursor. The former material was obtained by conventional solid-state reaction of Co_3O_4 with

Na_2CO_3; due to the use of the nanosized Co_3O_4 precursor, the thermal treatment in air was performed for a relatively short time. The latter was produced by using NaOH in water as the Na source, followed by calcination of the dried precursors. The structural and morphological features of the cobalt oxide precursor and of both mixed-oxides were investigated in detail and showed the presence of well crystallized particles with a controlled morphology and nanometric or sub-micrometric size.

The electrochemical characterization revealed good kinetics of the de-intercalation–intercalation processes with a very small ohmic drop and excellent energy efficiency. In particular, $Na_{0.71}CoO_2$ with 2D platelet structure exhibited the best behavior with a stable discharge specific capacity of 120 and 80 mAh g^{-1} at 5 and 40 mA g^{-1}, respectively, in the range 2.0–3.9 V. These performances are significantly better than those of current state-of-the-art Na_xCoO_2-based batteries and therefore make this material suitable to develop highly efficient Na-ion batteries.

Experimental

Chemicals

Cobalt carbonate hydrate ($CoCO_3 \cdot xH_2O$ 99.998%), sodium hydroxide (NaOH, $\geq$ 98%), hydrogen peroxide solution (H_2O_2, 30%) and sodium carbonate anhydrous (Na_2CO_3, 99.999%) were all purchased from Aldrich and used as received without further purification.

Preparation of $Na_{0.71}CoO_2$ samples

The cathode materials have been prepared by a two-step approach involving the hydrothermal synthesis of Co_3O_4 nanocrystals and the successive reaction either with NaOH (sample I) or with Na_2CO_3 (sample II) to form $Na_{0.71}CoO_2$ powders.

Hydrothermal synthesis of Co_3O_4 nanopowders

In a typical synthesis of Co_3O_4 nanocrystals, 0.67 g of $CoCO_3 \cdot xH_2O$ were slowly added to an aqueous solution of 3 M sodium hydroxide (NaOH) at room temperature and under vigorous stirring. The resulting pink suspension of $Co(OH)_2$ was stirred for 15 minutes and then oxidized by adding drop wise 2 mL of a hydrogen peroxide solution (H_2O_2 30%). The obtained dark brown suspension was stirred for 15 minutes and then transferred into a 60 mL Teflon lined stainless steel autoclave and heated to 180 °C for 2 h in an oven. The autoclave was cooled in air and, after decantation, Co_3O_4 nanopowders were recovered by centrifugation, washed with water and acetone and finally dried under vacuum ($p < 10^{-2}$ mbar).

Preparation of $Na_{0.71}CoO_2$ (I)

Na_2CO_3 and hydrothermally obtained Co_3O_4 nanocrystals were mixed thoroughly and the mixture was subjected to thermal annealing in air at 800 °C for 16 h. According to the sodium volatility, the initial 5 wt% excess of Na_2CO_3 was used.

Preparation of $Na_{0.71}CoO_2$ (II)

Co_3O_4 hydrothermal powders were suspended under ultrasound in 10 mL of 0.3 M NaOH aqueous solution. The solvent was then removed on a rotary evaporator and the wet powders were dried in air at 60 °C, then calcined at 800 °C for 16 hours.

Characterization methods

The X-ray diffraction (XRD) patterns of hydrothermally obtained Co_3O_4 nanocrystals and $Na_{0.71}CoO_2$ powders were collected with a Bruker D8 Advance diffractometer (Cu Kα radiation) operating in the range 10–70° 2θ (2θ step 0.020°, counting time 2 s per step).

Scanning electron microscopy (SEM) measurements were performed by a Vega TS5136 XM Tescan microscope in a high vacuum configuration. The electron beam excitation was 30 kV at a beam current of 25 pA, and the working distance was 12 mm. In this configuration the beam spot was 38 nm. Prior to SEM analysis, samples were gold-sputtered.

High-resolution transmission electron microscopy (HRTEM) and electron diffraction (SAED) measurements were performed using a Jeol 3010 apparatus operated at 300 kV with a high-resolution pole piece (0.17 nm point-to-point resolution) and equipped with a Gatan slow-scan 794 CCD camera. The powders were suspended in isopropanol, and a 5 μL drop of this suspension was deposited on a holey carbon film supported on a 3 mm copper grid for TEM investigation.

The elemental composition was determined by Atomic Absorption Spectroscopy (AAS, PerkinElmer 100). Roughly 10 mg of powder were dissolved in acid solution (HCl 37%/HNO_3 63% = 6 : 1) and the composition was determined from the Na/Co ratio (assuming no oxygen deficiencies).

The electrochemical characterization was carried out using three electrode Swagelok cells. Active material electrodes were fabricated by mixing the powdered $Na_{0.71}CoO_2$ with carbon black (SuperP MMM Carbon) and an organic binder (PVDF-HF, Solvay) in an 8 : 1 : 1 weight ratio. The mixture was dispersed in *n*-methyl-pyrrolidone (NMP) to obtain dense slurry which was casted directly on the stainless steel current collector of the Swagelok cell. The active material load was around 3 mg cm^{-2}. Metallic sodium discs were pasted at the top of the two different current collectors, and they were used as reference and counter electrodes. All the potentials are reported *versus* the couple Na^+/Na. The small gap among the electrodes was filled with the electrolyte which was $NaClO_4$ (1 M) in propylene carbonate. This cell arrangement minimizes the number of materials used in cell assembling; thus the result is directly relatable to the material performances. For this reason, the cell was kept in an Ar filled glove box ($[O_2] < 1$ ppm) during all the measurements. Both cyclic voltammetries (CV) and galvanostatic cycling with potential limitation (GCPL) were performed. CVs were carried out at 0.1 mV s^{-1} in the 2.0–4.0 V potential range. GCPL were performed at different current rates using 2.0 and 3.9 V as low and high cut off voltage, respectively. The gravimetric current density values are reported as the corresponding C rates, using the value of 249.9 mAh g^{-1} as theoretical specific capacity for the intercalation and de-intercalation of 1 mol of Na^+ ions in Na_xCoO_2 where $x = 0.71$ is the initial composition (1 C corresponds to 249.9 mA g^{-1}).

Results and discussion

Structural and morphological characterization

Fig. 1 shows the XRD patterns of hydrothermally obtained Co_3O_4 nanocrystals (a) and of $Na_{0.71}CoO_2$ powders (b and c).

In particular, the diffraction peaks of both samples I and II have been indexed based on the hexagonal crystal system with space group $P6_3/mmc$ and lattice parameters a = 2.833 Å and c = 10.880 Å, which agree with the values reported for the phase γ-$Na_{0.71}Co_{0.96}O_2$ (JCPDS file no. 30-1182, see the structure in Fig. 1). It is interesting to note that the $Na_{0.71}CoO_2$ phase was obtained by a relatively short thermal treatment (16 h in air instead 24 h at 850 °C under oxygen flow as reported in ref. 20), due to the nanometric morphology of the Co_3O_4 precursor.

The distance between the two cobalt oxide layers is about 5.45 Å. The Co–O distance in γ-$Na_{0.71}Co_{0.96}O_2$ (1.941 Å) is very similar to those in $LiCoO_2$,[25,26] but the Na–O distance (2.381 Å) is greater than the Li–O one. Therefore, the larger Na^+ ions have suitable space to diffuse through layered structures. This is not the case of rigid poly-anionic systems such as poly-phosphate ($FePO_4$), where phosphate tetrahedrons bridge the FeO_6 octahedrons creating a stable three dimensional structure where the alkaline ions have to diffuse through.

TEM and HRTEM micrographs of Co_3O_4 nanocrystals are reported in Fig. 2. No internal pores or amorphous surface layers were detectable. Particles are single nanocrystals, with pronounced faceting, organized in irregular aggregates (Fig. 2a). The nanoparticles mainly show elongated prismatic shape with the major dimension ranging from 140 to 190 nm and the minor from 45 to 70 nm (see Fig. 2b and c). High-resolution (HRTEM) image of Co_3O_4 nanocrystals (Fig. 2d) evidences that the lattice fringes have a spacing of 0.290 nm, which matches the interplanar distance of the (220) plane of the cubic cobalt oxide (JCPDS file no. 42-1467).

Fig. 3 summarizes the SEM micrographs performed on both $Na_{0.71}CoO_2$ materials. Sample I (Fig. 3a and c) displays crystals with 2D platelet shape, entirely exposed sheet edges, exposed flat surfaces, thickness ranging from 250 to 500 nm and edge to edge distance (length) centered at 3.2 μm (see inset of Fig. 3a). In some micrometric zones of the sample, several hexagonal particles can be easily detected (see Fig. 3c). SEM micrographs of $Na_{0.71}CoO_2$ sample II (Fig. 3b and d) instead show microcrystals with irregular shape, undefined exposed surfaces, higher length and broader length distribution (inset of Fig. 3b).

From the EDX analysis (Fig. S1, ESI†) carried out over about 40 different particles of both the obtained materials, the Na/Co atomic ratio resulted is 0.71, in agreement with the chemical composition of γ-$Na_{0.71}Co_{0.96}O_2$ phase. Accordingly, elemental analyses performed by atomic absorption spectroscopy (AAS) revealed that the Na/Co molar ratio is 0.69 for $Na_{0.71}CoO_2$ (I) and about 0.74 for $Na_{0.71}CoO_2$ (II), confirming the successful synthesis of γ-$Na_{0.71}Co_{0.96}O_2$.

In accordance with the SEM images, TEM investigation performed on $Na_{0.71}CoO_2$ (I) showed aggregates of micrometric particles with hexagonal shape (Fig. 4a).

At higher magnification, crystals appear well faceted (Fig. 4b and c) and free of surface impurities or secondary

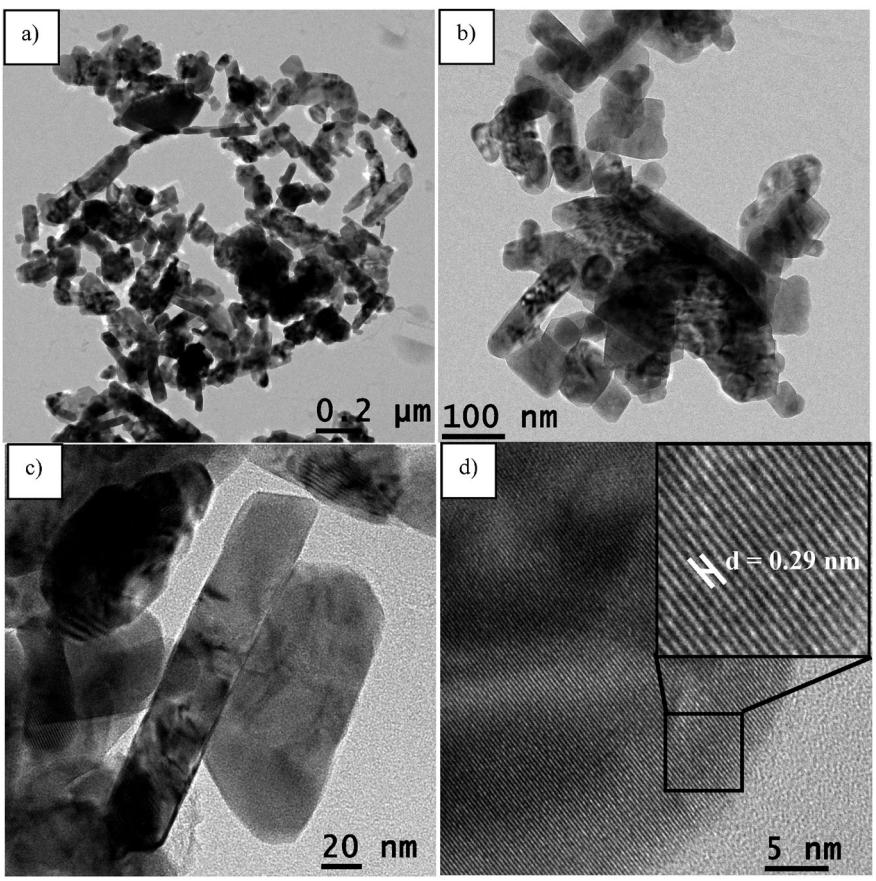

Fig. 2 TEM (a–c) and HRTEM (d) images of hydrothermally obtained Co_3O_4 nanocrystals. Details on crystallographic planes detected are showed in the inset of (d).

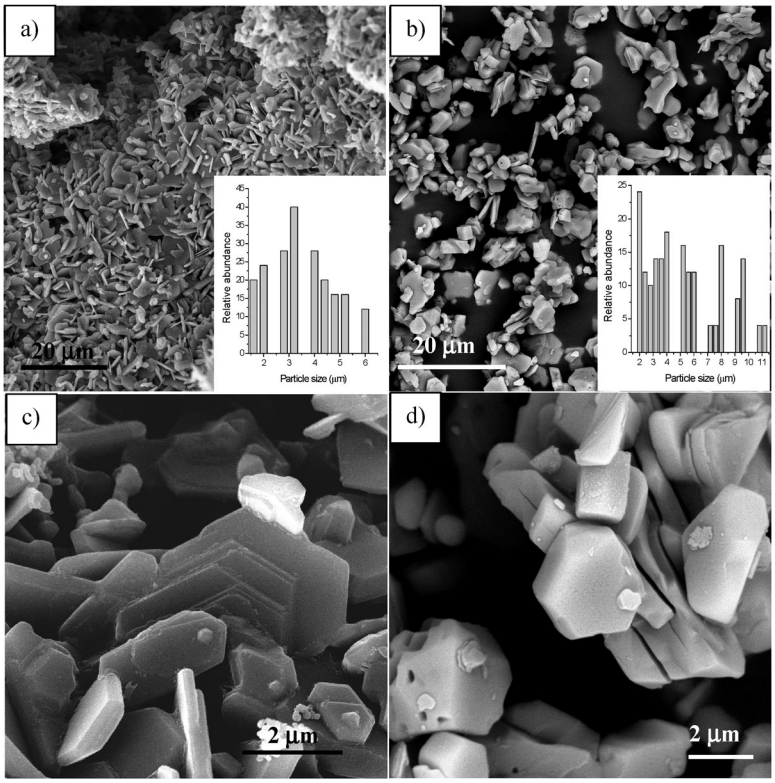

Fig. 3 SEM micrographs (a and c) of $Na_{0.71}CoO_2$ sample I and (b and d) $Na_{0.71}CoO_2$ sample II. Insets in (a) and (b) report the particle-size distribution evaluated by measuring the length (edge to edge distance) of ~200 particles in $Na_{0.71}CoO_2$ (I) and $Na_{0.71}CoO_2$ (II), respectively.

phases, as assessed by the SAED pattern collected on an oriented microcrystal (inset in Fig. 4c). HRTEM images taken on a platelet of $Na_{0.71}CoO_2$ (I) (Fig. 4d) confirmed the layered structure of the product. In particular, the figure inset shows lattice fringes with a spacing of 0.539 nm which corresponds to the distance between two adjacent CoO_2 layers in the hexagonal $Na_{0.71}Co_{0.96}O_2$ structure.[22] Some edge and screw dislocations are detectable in the sheets, probably related with the non-stoichiometric molar ratio of Na in the obtained phase.

TEM images of $Na_{0.71}CoO_2$ (II) are reported in Fig. 5. In line with the SEM investigation, the sample shows microcrystals with irregular shape and size, organized in large aggregates.

Electrochemical characterization

The cyclic voltammetries of both $Na_{0.71}CoO_2$ phases at a scan rate of 0.1 mV s^{-1} are reported in Fig. 6. From the profiles it is confirmed that the $Na_{0.71}CoO_2$ material has an electrochemical behavior showing several reaction voltages. This case is quite common in layered sodium ion intercalation compounds, for example $Na_4Mn_9O_{18}$ shows at least 7 different current peaks when the potential is swept between 2.0 and 3.7 V *vs.* Na.[13] During the anodic scan the current voltage profiles of the two materials (I and II) are similar, but in the cathodic branch $Na_{0.71}CoO_2$ (I) shows much better peak resolution indicating faster electrode kinetics. In fact, for each peak couple of $Na_{0.71}CoO_2$ (I) a potential difference of about 80 mV is observed, pointing out that the kinetics of the electrochemical process is under diffusional control of the Na^+ ion in the structure, as a result of the high electronic conductivity of the phase.[27] The complexity of the CV profile can be explained in terms of structure–properties relationships: in fact the change in Na^+ amount induces different cation distribution in the layer changing the energy required for the de-intercalation–intercalation process. The scanned 2–4 V potential range can be split into three different regions (from 2.2 to 2.8 V, from 2.8 to 3.4 V, and from 3.6 to 4.0 V respectively) separated by the two large current drops around 2.8–2.9 V and 3.4–3.6 V, respectively. The former drop is relatable to a phase transition between the solid solution regions (potential < 2.8 V) and the biphasic domain (potential > 2.8 V) observed by *in situ* XRD measurements,[21] while no explanation has been reported for the latter current decrease.

Fig. 7a shows the characteristic multistep charge–discharge profiles of both materials obtained at the lowest current rate (C/50, 5.00 mA g^{-1}). Profiles are in agreement with the CV measurements and the curve shown in the literature[21] performed at much lower current value (C/100). In fact, a series of potential drops are present corresponding to the current decreases in the CV. Even at this low current rate, the two phases display quite different charge capacities with values of 135 and 105 mAh g^{-1} for $Na_{0.71}CoO_2$ (I) and $Na_{0.71}CoO_2$ (II), respectively.

The close potential values between the charge and the discharge lines in both $Na_{0.71}CoO_2$ materials is a proof of the very good electronic conductivity of the phase having a very small ohmic drop. The coulombic efficiency at the end of the discharge is 95% for both materials. A close look at the curve reveals that most of the capacity loss lies in the 3.7–3.9 V potential range, wherein the electrolyte decomposition may take place. At this low current rate more than 120 mAh g^{-1} can be delivered by the $Na_{0.71}CoO_2$ (II) in the discharge; thus,

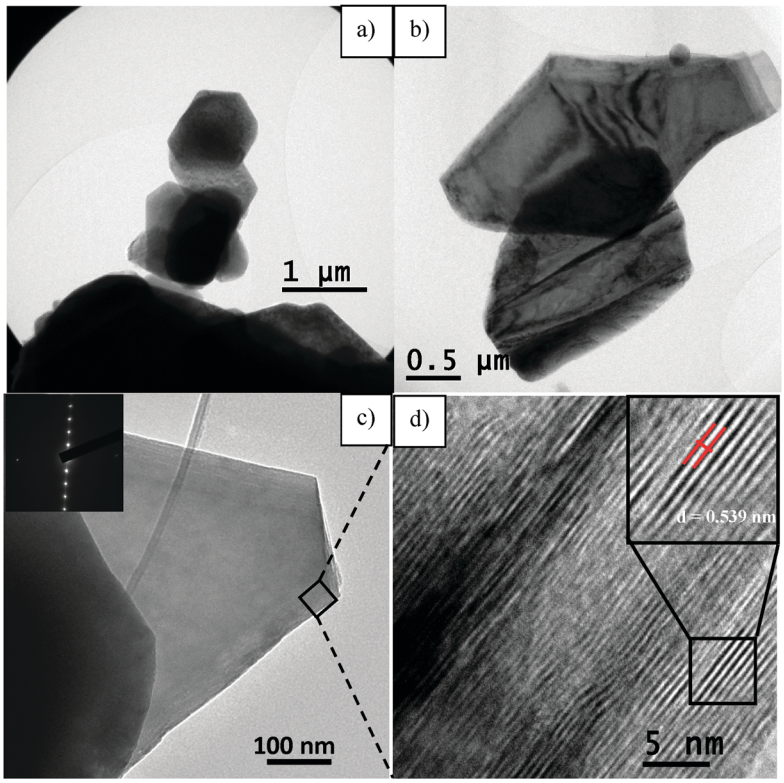

Fig. 4 TEM (a–c) and HRTEM (d) images of $Na_{0.71}CoO_2$ (I) powders. Dislocations in the layered structures are marked by the dashed circles. Inset in (c) SAED pattern collected on an oriented crystal.

in order to determine the electrode rate capability, increased current values were applied for several cycles. The profiles are reported in Fig. 7b, where good kinetic properties of the system were observed until the current value of 20.0 mA g^{-1}

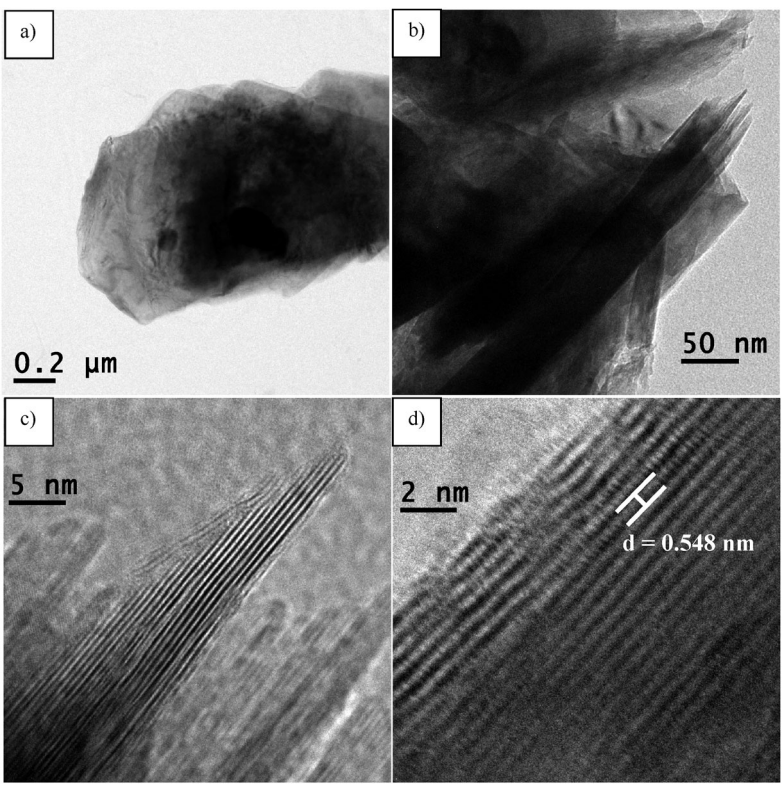

Fig. 5 TEM (a and b) and HRTEM (c and d) images of $Na_{0.71}CoO_2$ (II) microcrystals.

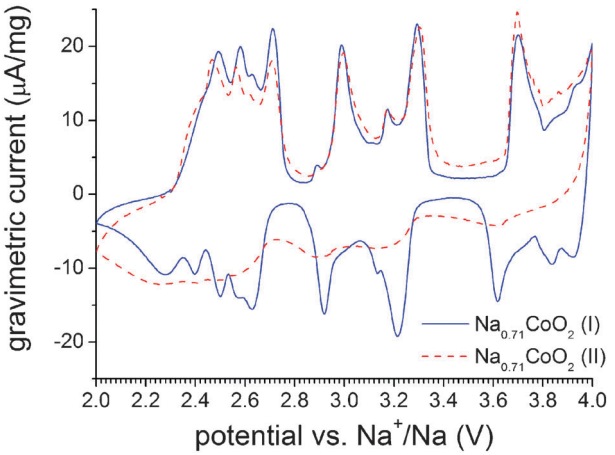

Fig. 6 CVs profile of the $Na_{0.71}CoO_2$ phases in 1.0 M $NaClO_4$ in PC at 0.1 mV s^{-1}.

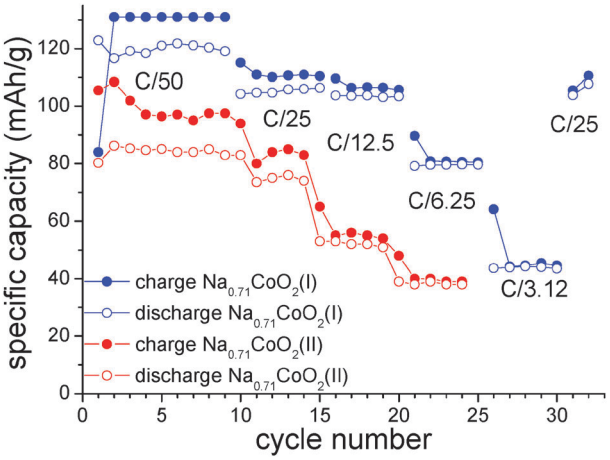

Fig. 8 Charge/discharge and Coulomb efficiency values of $Na_{0.71}CoO_2$ phases in 1.0 M $NaClO_4$ in PC at different current rates (1 C = 249.9 mA g^{-1}).

(capacity higher than 100 mAh g^{-1}). Above this value the specific capacity rapidly fades to 80 and 45 mAh g^{-1} which were obtained at 40.0 and 80.0 mA g^{-1}, respectively. The stoichiometry of the deinserted phase (V = 3.9) was estimated as about $Na_{0.4}CoO_2$, which is close to the instability limit of $LiCoO_2$. However, the larger oxygen to oxygen distance along the c axis should allow a wider deintercalation range due to a weaker Coulomb interaction between the anion slabs.

The materials cycling properties are better reported in terms of specific capacity as a function of the cycle number at the various current rates (Fig. 8). In the case of $Na_{0.71}CoO_2$ (I), the specific capacity reaches a plateau after few cycles at each new current rate. Thus, the specific capacities discussed in Fig. 7b are representative values for the corresponding current. Moreover, if the rate is lowered to C/25 after five cycles at C/3.12, the previously observed capacity is obtained again, as a proof that if the material works close to its kinetic limit, no irreversible degradation takes place.

The Coulomb efficiency increases with the increase of the current rate because the longer the time the system stays at high potential the higher the irreversible oxidative capacity becomes due to the electrolyte decomposition.[21] A value higher than 98% is observed for the charge efficiency at both C/6.25 and C/3.12. The specific capacities of $Na_{0.71}CoO_2$ (II) are always lower, and a net decrease in performances is observed at C/12.5 rate where values of 55 mAh g^{-1} are delivered by the phase. Both the potential profiles and the specific capacities are comparable with those of other layered materials reported in the literature. In fact, $Na_4Mn_9O_{18}$ and $Na_{1.0}Li_{0.2}Ni_{0.25}Mn_{0.75}O_\delta$ displayed the multistep voltage behavior and a specific capacity slightly above 100 mAh g^{-1}.[13–16] The only isostructural, single reaction voltage material (3.0 V) reported in the literature is $NaCrO_2$ having a specific capacity of 110 mAh g^{-1}.[17]

Both CV profiles (Fig. 6) and galvanostatic measurements (Fig. 7) converge in demonstrating that the phase obtained by the direct solid state reaction of Co_3O_4 with Na_2CO_3 has better kinetic properties with respect to the phase obtained using NaOH as the Na^+ precursor. Since the crystalline structure is the same (see the XRD profiles in Fig. 1), it is reasonable to suggest that the material morphology plays a relevant role in determining the electrochemical properties. Two main differences can be evidenced between the material morphologies: the particle thickness, since the $Na_{0.71}CoO_2$ (I) particles are much thinner (platelet shape) with respect to $Na_{0.71}CoO_2$ (II), and the particle length distributions (based on the edge to edge distance in platelets) as reported in the insets

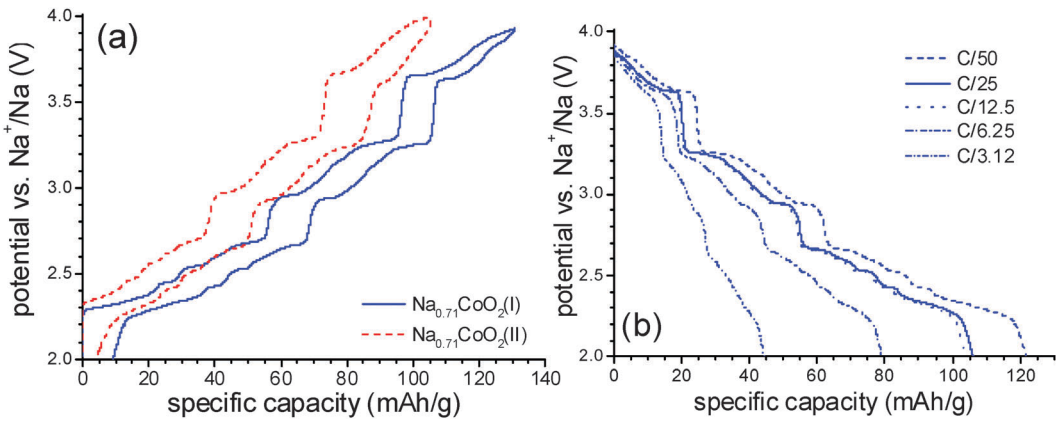

Fig. 7 (a) Charge/discharge curves of $Na_{0.71}CoO_2$ phases in 1.0 M $NaClO_4$ in PC solution at 0.1 mV s^{-1} at C/50 current rate (5th cycle), and (b) discharge current obtained at different current rates (1 C = 249.9 mA g^{-1}) for $Na_{0.71}CoO_2$ (II).

of Fig. 3a and b. TEM images and XRD of $Na_{0.71}CoO_2$ (I) also indicate that the platelets are oriented with the shortest direction (thickness) along the *c* axis, perpendicularly to the Na^+ layers wherein the ionic diffusion takes place. Therefore the particle thickness is not expected to affect the ionic diffusion paths in the material, which are instead controlled by the particle length. A smaller edge to edge distance thus provides shorter diffusion paths for the sodium ions in the crystalline structure and the improved electrochemical behavior of $Na_{0.71}CoO_2$ (I) can be ascribed to the narrower size distribution, compared to the broader one observed in $Na_{0.71}CoO_2$ (II).

Conclusions

Two $Na_{0.71}CoO_2$ phases with different morphologies have been obtained by solid state reaction of nanosized Co_3O_4 with a suitable Na^+ ion precursor. The key point for the preparation of highly crystalline mixed oxide is the use of a suitable nanosized Co_3O_4 precursor prepared by hydrothermal synthesis. The two mixed oxides, obtained from Na_2CO_3 ($Na_{0.71}CoO_2$ (I)) and from NaOH ($Na_{0.71}CoO_2$ (II)), respectively, have the same hexagonal P2 crystal structure but different morphologies: $Na_{0.71}CoO_2$ (I) particles are smaller, with length distribution centered around 3 μm, instead the particles of $Na_{0.71}CoO_2$ (II) are larger (many crystals have edge to edge distances above 10 μm), and have broader length distribution. These morphological features significantly affect the electrochemical behavior of the materials. In fact, $Na_{0.71}CoO_2$ (I) has better kinetic properties as pointed out by the CV profiles and by the specific capacity values obtained at different current rates. The improved kinetic properties have been attributed mainly to the reduced particle length which implies shorter diffusion paths for the Na-ion intercalation and extraction in the crystalline structure. Although battery materials should have only one reaction voltage for a more efficient energy conversion, the P2 $Na_{0.71}CoO_2$ phase has an electrochemical behavior involving several redox processes. However, this peculiar electrochemical feature would allow a better control of the cell state of charge which is becoming a fundamental aspect in the design and fabrication of large battery stacks for high power applications.

The $Na_{0.71}CoO_2$ (I) material showed a stable discharge specific capacity of 120, 105, and 80 mAh g^{-1} at 5, 20, and 40 mA g^{-1}, respectively, in the potential range 2.0–3.9 V. These performances are promising and significantly better than those of current state-of-the-art of Na_xCoO_2-based batteries.

In conclusion, it has been demonstrated that the reversible intercalation and deintercalation of Na^+ ions at room temperature is favored in easy obtainable $Na_{0.71}CoO_2$ layered compounds which are suitable prototypes for future development of positive electrodes in high-performance ion batteries.

Acknowledgements

The Milan group gratefully acknowledges Dr Paolo Gentile for the SEM images and Dr Angeloclaudio Nale for the XRD experiments. The authors also personally thank Monica Resnati and Luca Malchiodi for their support in the experimental work.

Notes and references

1 J. M. Tarascon, *Nat. Chem.*, 2010, **10**, 510.
2 http://worldlithium.com/An_Abundance_of_Lithium_1html.
3 http://www.lithiumsite.com/Lithium_Market.html.
4 M. Armand and J. M. Tarascon, *Nature*, 2008, **451**, 652.
5 V. Palomares, P. Serras, I. Villaluenga, K. B. Hueso, J. C. Gonzalez and T. Rojoab, *Energy Environ. Sci.*, 2012, **5**, 5884.
6 S. P. Ong, V. L. Chevrier, G. Hautier, A. Jain, C. Moore, S. Kim, X. Ma and G. Ceder, *Energy Environ. Sci.*, 2011, **4**, 3680.
7 K. Trad, D. Carlier, L. Croguennec, A. Wattiaux, B. Lajmi, M. B. Amara and C. Delmas, *J. Phys. Chem. C*, 2010, **114**, 10034.
8 Z. Jian, L. Zhao, H. Pan, Y. S. Hu, H. Li, W. Chen and L. Chen, *Electrochem. Commun.*, 2012, **14**, 86.
9 K. Trad, D. Carlier, L. Croguennec, A. Wattiaux, M. B. Amara and C. Delmas, *Chem. Mater.*, 2010, **22**, 5554.
10 P. Moreau, D. Guyomard, J. Gaubicher and F. Boucher, *Chem. Mater.*, 2010, **22**, 4126.
11 K. T. Lee, T. N. Ramesh, F. Nan, G. Botton and L. F. Nazar, *Chem. Mater.*, 2011, **23**, 3593.
12 F. Sauvage, L. Laffont, J.-M. Tarascon and E. Baudrin, *Inorg. Chem.*, 2007, **46**, 3289.
13 Y. Cao, L. Xiao, W. Wang, D. Choi, Z. Nie, J. Yu, L. V. Saraf, Z. Yang and J. Liu, *Adv. Mater.*, 2011, **23**, 3155.
14 J. F. Whitacre, A. Tevar and S. Sharma, *Electrochem. Commun.*, 2010, **12**, 463.
15 M. M. Doeff, M. Y. Peng, Y. Ma and L. C. De Jonghe, *J. Electrochem. Soc.*, 1994, **141**, L145.
16 D. Kim, S. H. Kang, M. Slater, S. Rood, J. T. Vaughey, N. Karan, M. Balasubramanian and C. S. Johnson, *Adv. Energy Mater.*, 2011, **1**, 333 C.
17 S. Komaba, C. Takei, T. Nakayama, A. Ogata and N. Yabuuchi, *Electrochem. Commun.*, 2010, **12**(3), 355.
18 C. Delmas, J.-J. Braconnier, C. Fouassier and P. Hagenmuller, *Solid State Ionics*, 1981, **3,4**, 165.
19 S. Kikkawa, S. Kiyazaki and M. Koizumi, *J. Power Sources*, 1985, **14**, 231.
20 L. W. Shacklette, T. R. Jew and L. Townsend, *J. Electrochem. Soc.*, 1988, **135**, 2669.
21 R. Berthelot, D. Carlier and C. Delmas, *Nat. Mater.*, 2011, **10**, 74.
22 C. Delmas and C. Fouassier, *Physica B+C (Amsterdam)*, 1980, **99**, 81.
23 Y. Ma, M. M. Doeff, S. J. Visco and L. C. de Jonghe, *J. Electrochem. Soc.*, 1993, **140**, 2726.
24 A. Bhide and K. Hariharan, *Solid State Ionics*, 2011, **192**, 360.
25 H. J. Orman and P. J. Wiseman, *Cryst. Struct. Commun.*, 1984, **40**, 12.
26 Y. Takahashi, Y. Gotoh and J. Akimoto, *J. Solid State Chem.*, 2003, **172**, 22.
27 A. Mendiboure, C. Delmas and P. Hagenmuller, *J. Solid State Chem.*, 1985, **57**, 323.

